Nanostructured Organic–Inorganic Hybrid Films Prepared by the Sol–Gel Method from Self-Assemblies of PS-*b*-PAPTES-*b*-PS Triblock Copolymers

Cé Guinto Gamys,[1,2,3] Emmanuel Beyou,[1,2,3] Elodie Bourgeat-Lami,[1,2,4] Pierre Alcouffe,[1,2,3] Laurent David[1,2,3]

[1]Université de Lyon, Lyon F-69003, France
[2]Université Lyon 1, Villeurbanne, F-69622, France
[3]CNRS UMR 5223, Ingénierie des Matériaux Polymères: Laboratoire des Matériaux Polymères et Biomatériaux, IMP@Lyon1, 15 Boulevard Latarjet, Villeurbanne F-69622, France
[4]CPE Lyon, CNRS, UMR 5265, Laboratoire de Chimie, Catalyse, Polymères et Procédés (C2P2), LCPP Group, 43, Bd. du 11 Novembre 1918, Villeurbanne F-69616, France

Correspondence to: E. Beyou (E-mail: beyou@univ-lyon1.fr)

Received 13 May 2011; accepted 27 June 2011; published online 22 July 2011
DOI: 10.1002/pola.24861

ABSTRACT: ABA-based triblock copolymers of styrene as block ends and gelable 3-acryloxypropyltriethoxysilane (APTES) as the middle block were successfully prepared through nitroxide-mediated polymerization (NMP). The copolymers were bulk self-assembled into films and the degree of phase separation between the two blocks was evaluated by differential scanning calorimetry (DSC). Their morphology was examined through small angle X-ray scattering (SAXS) and transmission electron microscopy (TEM), whereas the mechanical properties of the corresponding cross-linked self-assembled nanostructures were characterized by dynamic mechanical analysis (DMA). Acidic treatment of the triblock copolymers favored the hydrolysis and condensation reactions of the APTES-rich nanophase, and induced a mechanical reinforcement evidenced by the increase of storage modulus values and the shift of the glass transition temperature to higher temperatures due to confinement effects. In addition, the lamellar structure of the hybrid films was retained after the removal of the organic part by calcination. © 2011 Wiley Periodicals, Inc. J Polym Sci Part A: Polym Chem 49: 4193–4203, 2011

KEYWORDS: block copolymers; bulk self-assembly; crosslinking; kinetics (polym.); living radical polymerization (LRP); mechanical properties; morphology; SAXS; sol–gel; triblock copolymers

INTRODUCTION In recent years, the elaboration of silica-based nanomaterials has received a great deal of attention[1–11] owing to their potential applications in many fields. For instance, particles with a magnetic core and a mesoporous silica shell have been used as magnetic resonance and fluorescence imaging agents, and as drug delivery vehicles, thus making them novel candidates for simultaneous cancer diagnosis and therapy.[12] Both hollow and core–shell organosilica nanoparticles with varying silica contents have been synthesized by using supramolecular templating approaches.[7,8] Moreover, a wide range of nanomaterials with controlled shape and size can be produced by cross-linking preformed block copolymer assemblies. Through a judicious choice of monomer type, relative block lengths, and experimental conditions, block copolymers can readily self-assemble to form vesicles and spherical micelles with tailored chemical, physical, or biological properties.[13,14] On the other hand, the sol–gel process,[15] which relies on base- or acid-catalyzed hydrolysis and condensation reactions of metal alkoxides or organically modified metal alkoxide precursors, is frequently used to obtain organic–inorganic hybrid materials.[16–18] The structure and final morphology of these hybrid materials are highly dependent on the nature of the organic moiety. Recently, gelable poly(3-triethoxysilyl)propylmethacrylate (PTEPM)-based block copolymers were self-assembled in solution[19–22] and in bulk[23–26] generating spherical micelles and vesicles in solution, and well-defined lamellar, cylindrical, and spherical morphologies in bulk depending on the composition of the copolymer. For example, by changing the molecular weight fraction of a gelable PTEPM block in a PTEPM-*b*-P2VP diblock copolymer from 25.6 to 6.6%, Zhang et al.[24] reported the formation of three different microphase-separated morphologies, that is, lamella, hexagonally packed cylinders, and liquidlike spheres. These morphologies were then successfully frozen by an *in situ* sol–gel reaction of the triethoxysilyl groups to form well-defined hairy nanohybrids.

Our group recently reported the synthesis of poly(3-acryloxypropyltriethoxysilane)-*b*-poly(styrene) (PAPTES-*b*-PS) diblock

Additional Supporting Information may be found in the online version of this article.

copolymers of various compositions and molecular weights. These diblock copolymers were subsequently self-assembled into spherical micelles with a PS core and a PAPTES corona in a mixture of dioxane and methanol.[16] Contrary to all previous works, we performed the cross-linking of the PAPTES corona in acidic medium. Surprisingly, most of the works in this topic deal with diblock copolymers although it is well known that triblock terpolymers form a larger variety of nanostructures.[27] Indeed, a great number of well-defined nano-objects can be generated by using multiblock copolymers. For instance, ABC triblock terpolymers with a cross-linkable segment as the middle block were recently synthesized.[28–35] Photoinduced cross-linking was used to form polymer fibers with poly(acrylic acid) cores and poly(butyl methacrylate) coronas[33] while Chen and coworkers[36,37] reported the formation of an organic/inorganic hybrid nanoplate with a sandwichlike structure after *in situ* self-gelation of PTEPM microdomains. They obtained microphase separation with a lamellar morphology by bulk casting and annealing a solution of PTEMP-*b*-PS-*b*-P2VP triblock terpolymer in tetrahydrofuran (THF).[37] Finally, organosilica nanoshells with a large internal cavity were prepared through the cross-linking of triethoxysilyl-terminated poly(ethylene glycol)-*b*-poly-(propylene oxide)-*b*-poly(ethylene oxide) triblock terpolymers by using a miniemulsion process.[38] In addition, it has been found that ABA (or BAB) triblock copolymers display lower conformational entropy of their ordered state than that of an AB diblock copolymer with the same chain length and composition because the two block junctions are located at a domain boundary.[39,40] As a consequence, the disordered state of triblock copolymer melts is more stable than that of diblock copolymers. However, to the best of our knowledge, the utilization of ABA triblock copolymers with a gelable group [such as 3-acryloxypropyltriethoxysilane (APTES) in the central block or with PAPTES block ends], to generate self-assembled thin films, has not yet been investigated.

In this article, we investigate the bulk self-assembly of PS-*b*-PAPTES-*b*-PS triblock copolymers. For the first time, we describe the preparation of these triblock copolymers with various compositions and molecular weights by nitroxide-mediated polymerization (NMP). The degree of phase separation between the two blocks was evaluated by differential scanning calorimetry (DSC), whereas the mechanical properties of the corresponding cross-linked self-assembled nanostructures were characterized by dynamic mechanical analysis (DMA).

EXPERIMENTAL

Materials

3-Acryloxypropyl trimethoxysilane (APTMS, ABCR, 95% purity) was purified by distillation under reduced pressure. 3-Acryloxypropyltriethoxysilane (APTES) was synthesized by the alcoholysis of APTMS as reported elsewhere.[41] Styrene (Acros, 99% purity) was distilled under vacuum before use. The alkoxyamine initiator (styryl-DEPN) was prepared using a procedure described in the literature.[42] Anhydrous methanol (Acros, >99%), THF (Sigma-Aldrich, >99%), and toluene (Riedel-de Haen, >99%) were used as received.

Synthesis of PS Macroinitiators (PS-DEPN)

The polymerization was performed in a sealed ampoule under vacuum. Styryl-DEPN (49.7 mg, 1.2×10^{-1} mmol), styrene (10 g, 96.1 mmol), and toluene (14.95 g) were charged into a 50-mL Schlenk flask and the mixture was degassed by three freeze–evacuate–thaw cycles and then sealed under vacuum. Polymerization was carried out in an oil bath thermostated at 115 °C for different times. Then, toluene was evaporated and the crude product dispersed in THF was purified by precipitating into methanol three times and the recovered product was dried under vacuum. Samples were withdrawn during polymerization at specific time-intervals to follow the polymerization kinetics, as previously described.[18] The molecular weight and molecular weight distributions were determined by steric exclusion chromatography (SEC) analysis. The monomer conversion (X, %) was estimated by ^{1}H NMR analysis by comparing the peak areas of the protons of monomer and homopolymer. The theoretical number-average molecular weights ($M_{n_{theo}}$s) of PS were calculated from the monomer conversion and the styrene/styryl-DEPN molar ratio.

Synthesis of PS-*b*-PAPTES Macroinitiator Diblock Copolymers (PS-*b*-PAPTES-DEPN)

The polymerization was also performed in a sealed ampoule. A well-characterized PS-DEPN macroinitiator synthesized in a first step (see above) was used as macroalkoxyamine initiator of the PAPTES block. Typically, the PS macroinitiator (5.10 g, $M_{n_{SEC}} = 31{,}110$ g mol^{-1}, 1.64×10^{-1} mmol) was dissolved in a mixture of toluene (25.9 g) and APTES (24.9 g, 90.2 mmol). The solution was then degassed by three freeze–pump–thaw cycles, sealed under vacuum, placed in a thermostated oil bath at 115 °C, and allowed to react for different reaction times. The resulting copolymers were isolated and characterized as described previously for the PS homopolymer. The block composition was determined by ^{1}H NMR spectrum (Table 1).

Synthesis of PS-*b*-PAPTES-*b*-PS Triblock Copolymers

Similar to the experimental procedure described for the synthesis of the diblock copolymers, PS-*b*-PAPTES-*b*-PS triblock copolymers were synthesized from PS-*b*-PAPTES-DEPN macroinitiator diblock copolymers. The composition of the copolymer was determined by ^{1}H NMR analysis (Table 1).

Bulk Casting of PS-*b*-PAPTES-*b*-PS Triblock Copolymers

A solution of PS-*b*-PAPTES-*b*-PS triblock copolymer (50 mg mL^{-1}) in toluene was spread onto a clean Teflon plate with a syringe after filtration through a 0.45-μm membrane filter. The solvent was allowed to evaporate in a desiccator for 5 days. The resulting bulk sample (ca. 100–400 μm in thickness) was then dried for 12 h under vacuum at 60 °C and thermal annealing at 150 °C for 72 h under argon gave the triblock copolymer bulk sample with microphase separation.

Cross-Linking of the PAPTES Microdomains

The microphase-separated PS-*b*-PAPTES-*b*-PS films were immersed in an 1 mol L^{-1} aqueous solution of HCl for 24 h to carry out the sol–gel reaction of the PAPTES domains in acidic conditions. Then, the resulting cross-linked films were washed extensively with water to neutral pH and dried under vacuum at 60 °C for 24 h.

TABLE 1 Molecular Parameters of a Series of PS-*b*-PAPTES Macroinitiators and PS-*b*-PAPTES-*b*-PS Triblock Copolymers Obtained by DEPN-Mediated polymerization at 115 °C

Sample	Time (h)	Conversion[c] (%)	$M_{n_{theo}}$ (g mol^{-1})	$M_{n_{SEC}}$ (g mol^{-1})	$M_w/M_{n_{SEC}}$	Styrene:PS-*b*-PAPTES-DEPN	PS[a] (vol %)	d*n*/d*c*[b] (mL g^{-1})
PS_{272}-$PAPTES_{130}$-DEPN	16	26.1	64,300	59,990	1.18	–	43.6	0.100
PS_{272}-$PAPTES_{224}$-DEPN	32	44.9	90,250	83,310	1.21	–	31.0	0.077
PS_{272}-$PAPTES_{290}$-DEPN	64	58.1	108,470	101,250	1.30	–	25.7	0.064
PS_{272}-$PAPTES_{336}$-DEPN	128	67.2	121,000	110,800	1.32	–	23.0	0.056
$PS_{272}PAPTES_{130}PS_{268}$-DEPN	16	33.5	92,200	88,040	1.49	801	60.6	0.110
$PS_{272}PAPTES_{224}PS_{260}$-DEPN	24	32.7	117,300	110,700	1.52	795	46.8	0.095
$PS_{272}PAPTES_{290}PS_{293}$-DEPN	9	38.4	138,900	133,900	1.40	762	41.9	0.089
$PS_{272}PAPTES_{336}PS_{269}$-DEPN	9	35.0	149,000	139,300	1.48	769	37.3	0.081

[a] Calculated by ^{1}H NMR.
[b] Determined by interferometric refractometry.
[c] Calculated by ^{1}H NMR.

Characterization

^{1}H NMR (300 MHz) measurements were performed on a Bruker ALS 300 spectrometer at room temperature in $CDCl_3$. ^{29}Si solid-state NMR was performed on a Bruker DSX-300 apparatus operating at 59.63 MHz.

In the following and according to the conventional ^{29}Si NMR notation, silicon atoms surrounded by three oxygen atoms will be designated by T^{ij} were *i* corresponds to the number of Si—O—Si oxygen bridges and *j* to the number of hydroxyl groups.

SEC experiments were performed in THF at 25 °C and a flow rate of 0.5 mL min^{-1} using a system equipped with a Waters 410 differential refractometer and a Wyatt Technology mini-DAWN TREOS laser photometer as the light scattering detector. A 5-μm PLgel Mixed-D column was used and the absolute M_ns and molecular weight distributions (M_w/M_n) were determined using ASTRA for Windows with known specific refractive index increments (d*n*/d*c*).

The d*n*/d*c* values were determined using a NTF ScanRef interferometric refractometer at a wavelength of 633 nm. For PAPTES-*b*-PS copolymers, these values are in good agreement with those calculated on the basis of the composition of the copolymer given d*n*/d*c* values of 0.410 and 0.185 for the PAPTES and the PS blocks, respectively.

Specimens for transmission electron microscopy (TEM) analysis were observed at room temperature using a Philips CM-120 microscope (Philips Consumer Electronics BV, Eindhoven, The Netherlands) operating at 80 keV. Thin sections (50–100 nm) were obtained using a Leica Ultracut UCT ultramicrotome and a diamond knife at room temperature. The microtomed sections were observed without staining.

Scanning electronic microscopy (SEM) image on the calcined sample was obtained using a Hitachi S-800 microscope working at an accelerating voltage between 10 and 15 kV. DSC measurements were performed on a DSC 2920 apparatus (TA Instruments). The copolymers were dried at 70 °C before analysis and sealed in aluminum sample pans. The samples were scanned from -110 to 130 °C at a heating rate of 25 °C min^{-1}. The first heating scan was performed after decreasing the temperature from room temperature to –150 °C and then the sample was heated up to 150 °C. A second run was performed by cooling down the sample at the same rate and heating up again to 150 °C.

Thermogravimetric analysis (TGA) was carried out with a DuPont Instruments TGA 2950 thermobalance, controlled by a TC10A microprocessor. Samples were heated at 20 °C min^{-1} under a nitrogen flow (100 mL min^{-1}). The infrared spectra were recorded on a Fourier transform infra red (FTIR) Nicolet Magna 550 spectrometer.

Small angle X-ray scattering (SAXS) analysis was performed at the European Synchrotron Radiation Facility (ESRF, beam line BM2-D2AM, Grenoble, France). The use of a 2D-CCD detector (from Ropper Scientific) allowed us to record the scattering intensity in the scattering vector *q*-range from 0.008 to 0.3 A^{-1}. The incident energy was 16 keV and the sample-to-detector distance was close to 1 m. Silver Behenate was used as the standard for the *q*-range calibration. The radial average $I(q)$ was performed after correction of the distortion of the tapper, dark image contribution subtraction, and flat field normalization. The dynamic mechanical tests were carried out on a dynamic mechanical thermal analyzer (DMTA; MKIV, Rheometric Scientific) at a fixed frequency of 5.0 Hz and temperatures ranging from -120 to 170 °C (heating rate: 3.0 °C min^{-1}).

RESULTS AND DISCUSSION

Synthesis of PS-*b*-PAPTES-*b*-PS Triblock Copolymers

Nitroxide-mediated radical polymerization is a suitable method to ensure the synthesis of various polymer architectures, such as AB diblock, ABA triblock, and ABC triblock copolymers. Two different strategies are usually considered for the synthesis of ABA triblock copolymers. The first method is based on a three-step reaction by growing ABA triblock copolymers from monodirectional *N*-alkoxyamine initiators.[43] It requires isolation of the first block after the polymerization of a monomer and using it as macroalkoxyamine in the polymerization of a second monomer. Following

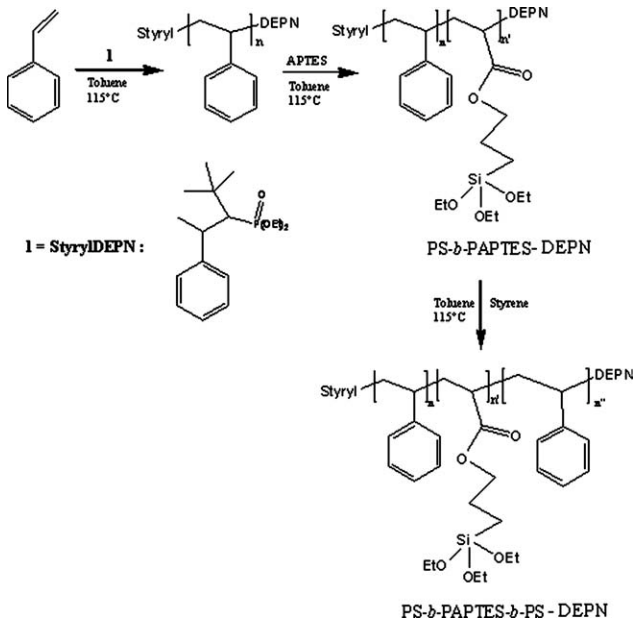

SCHEME 1 Scheme illustrating the synthesis of PS-*b*-PAPTES-DEPN and PS-*b*-PAPTES-*b*-PS-DEPN block copolymers.

polymerization, the resulting diblock copolymers are purified and polymerization is reinitiated by heating in the presence of the first monomer. An alternative is the use of bidirectional initiators capable of growing in two directions simultaneously.[44–46] This allows the three blocks to be grown in only two steps and ensures that both outside blocks are of the same length forming symmetrical ABA triblocks. Gnanou and coworkers[45] showed that well-defined PS-*b*-P*n*BuA-*b*-PS triblock copolymers containing 20–30% of PS could be generated on discontinuing the polymerization of styrene at moderate conversion (40%). However, they observed that the samples that derived from the dialkoxyamine exhibited larger polydispersity index than those issued from their monofunctional homologs (1.3–1.4 instead of 1.1). It was suggested that the growing monofunctional species can undergo irreversible recombination only once, whereas their difunctional homologs may participate in recombination more than one time leading to a slight broadening of the molar mass distribution.[45] Herein, we used the first strategy with a PS homopolymer synthesized in a first step and acting as macroinitiator agent in the synthesis of the second PAPTES block. Finally, the resulting PS-PAPTES diblock copolymers were allowed to react with styrene yielding PS-*b*-PAPTES-*b*-PS triblock copolymers (Scheme 1).

As shown in Table 1, well-defined PS-*b*-PAPTES-*b*-PS triblock copolymers with various chain lengths and compositions were successfully obtained. For clarity, only the polymerization kinetics of styrene from the PS_{272}-*b*-$PAPTES_{290}$-DEPN macroinitiator will be discussed in the following. As shown in Figure 1(a), the results indicate that the polymerization exhibits first-order kinetics with respect to monomer conversion. In addition, M_n evolved linearly with conversion while the polydispersity was lower than 1.5 and increased with increasing conversion [Fig. 1(b)]. The rather high polydispersity index may be attributed to some contamination with diblock species resulting from incomplete initiation by the PS-b-PAPTES-DEPN macroinitiator. There is also a close agreement between the experimental and theoretical M_ns. All these results confirm that the polymerization of styrene from the PS_{272}-*b*-$PAPTES_{290}$-DEPN macroinitiator exhibits all the characteristics of a controlled/"living" polymerization. Hence, contrary to Robin and Gnanou,[43] we found that sequential polymerization starting from a monofunctional alkoxyamine can lead to well-defined triblock copolymers without a too large amount of dead chains due to irreversible termination reactions during the three steps.

Formation and Characterization of PS-*b*-PAPTES-*b*-PS Films

It is well known that the compatibility of the individual blocks governs the aggregation properties of block copolymers in bulk.[47] DSC analysis of block copolymers provides information on the compatibility of the blocks and enables to determine their glass transition temperatures (T_gs). All DSC measurements were performed in the temperature range from −110 to 130 °C. As shown in the Supporting Information Figure S1, we observed two clearly distinct T_gs for all four block copolymers before hydrolysis–condensation reactions, with values close to those of the corresponding pure homopolymer segments (Table 2). In agreement with

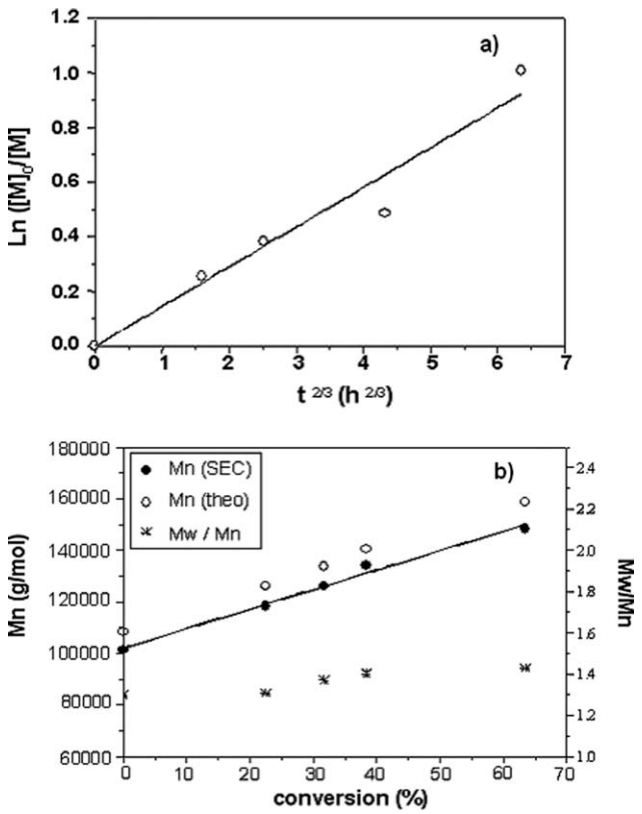

FIGURE 1 (a) First-order kinetics plot for the PS_{272}-*b*-$PAPTES_{290}$-DEPN-mediated stable free radical polymerization of styrene (initiator-to-styrene molar ratio = 762) and (b) evolution of the M_n and polydispersity index with conversion.

TABLE 2 Glass Transition Temperatures of a Series PS-*b*-PAPTES-*b*-PS Triblock Copolymers Before and After the Hydrolysis–Condensation Determined by DSC

				Before Hydrolysis–Condensation		After Hydrolysis–Condensation	
Sample	PS (vol %)	$M_{n_{SEC}}$ (g mol^{-1})	$M_w/M_{n_{SEC}}$	T_{g1} (°C)	T_{g2} (°C)	T_{g1} (°C)	T_{g2} (°C)
$PS_{272}PAPTES_{130}PS_{268}$	60.6	88,040	1.49	−70.6	102.9	–	109.2
$PS_{272}PAPTES_{224}PS_{260}$	46.8	110,700	1.52	−69.0	99.6	–	106.9
$PS_{272}PAPTES_{290}PS_{293}$	41.9	133,900	1.40	−68.8	98.7	–	104.3
$PS_{272}PAPTES_{336}PS_{269}$	37.3	139,300	1.48	−67.0	95.7	–	105.0

previous studies reporting the T_gs of triblock-based copolymers,[44,48] the T_g of the PS block (102.9 °C) in the PS-rich sample, is close to the T_g of pure PS (96 °C). With increasing the PAPTES soft block content, the T_g of the PS block decreases from 102.9 to 95.7 °C. This suggests that the pendant alkoxysilyl group has a plasticization effect on the triblock copolymers. As a matter of fact, the experimental glass transition temperature of the PAPTES block is close to −69 °C regardless of the polymerization degree (e.g., 130, 224, 290, and 336, respectively).

The self-assembled films were prepared by solvent casting after dissolving the PS-*b*-PAPTES-*b*-PS triblock copolymers in toluene and the nanophase-separated morphologies were observed by TEM. The TEM images of the four triblock copolymer films are shown in Figure 2. The dark areas in Figure 2 correspond to the PAPTES domains. An ordered structure of alternating PS and PAPTES lamellae is observed regardless of the composition of the copolymer. The latter lamellae morphology can be predicted by using the strong-segregation limit of the self-consistent field theory for block copolymer melts, which corresponds to the situation: $\chi N \gg 10$, where χ is the standard AB segment–segment Flory–Huggins interaction parameter and N is the overall degree of polymerization.[49] A lamellar morphology is shown to exist in AB diblock copolymers and ABA triblock copolymers within well-defined composition ranges and in particular for PS volume fractions varying from 0.34 to 0.62.[49] The average *d*-spacing was estimated from the electron micrographs to vary from 34.3 nm for the $PS_{272}PAPTES_{130}PS_{268}$ sample to 55.8 nm for the $PS_{272}PAPTES_{290}PS_{293}$ terpolymer (Table 3). Hence, it can be concluded that the *d*-spacing increases when increasing the M_n of the copolymer (e.g., 88,000 and 133,900 g mol^{-1}). This is in reasonable agreement in the literature for polybutadiene-*b*-polystyrene-*b*-polybutadiene triblock copolymers with molecular weight varying from 19,000 to 73,000 g mol^{-1}.[50] Helfand and Wasserman[50] and Hoffmann and coworkers[51,52] have carried out systematic studies on the effect of molecular weight on the structure parameter *d* of block copolymers and they found that *d* is proportional to the molecular weight for the strong-segregation regime. For example, Helfand and Wasserman[50] showed that $d \propto M^{0.643}$ for lamellar block copolymer microdomains. However, in our study, *d* does not increase linearly with the M_n of the copolymer. Indeed, the *d*-spacing value for the $PS_{272}PAPTES_{336}PS_{269}$ triblock copolymer (e.g., 51.4 nm) is lower than expected from the polymer molecular weight. Considering that some $PS_{272}PAPTES_{336}$-DEPN macroinitiator remains present into the films, these remaining macroinitiator may swell preferentially the soft PAPTES layer of the $PS_{272}PAPTES_{336}PS_{269}$ triblock copolymer because it displays a low PS volume content (23%) in comparison with the other macroinitiators. Thus, the interfacial area of the lamella increases and the PS layer thickness decreases to adjust to the extra interface, as discussed by Shen and coworkers[53] for blends of rod–coil–rod triblock copolymers and homopolymers.

The contamination of the PAPTES layer by the remaining diblock copolymer (with low PS content) may also explain that the lamellae edges are not as smooth as expected in Figure 2(c,d). However, the corresponding SEC trace does not permit to confirm it (Supporting Information Fig. S2).

The films were additionally characterized by SAXS (Fig. 3). The SAXS curves exhibit several correlation peaks or shoulders with a pattern of 1:2:3:4 in $PS_{272}PAPTES_{130}PS_{268}$, or $PS_{272}PAPTES_{224}PS_{260}$, and 1:2:3 in $PS_{272}PAPTES_{290}PS_{293}$ or $PS_{272}PAPTES_{336}PS_{269}$. All scattering diagrams are thus consistent with a lamellar morphology, as displayed in Figure 2. The second-order and fourth-order peaks are strongly attenuated and appear as a shoulder in triblock structures with longer PAPTES blocks, whereas a well-defined correlation peak can be observed with shorter PAPTES blocks. This could be related to a more disordered lamellar organization with a larger distribution of the width of the PAPTES lamellae (see the irregular structures for darker lamellae in Fig. 2), whereas the shorter PAPTES blocks induce thinner but a more regular lamellar organization in the investigated annealing conditions. The average *d*-spacings, calculated from the primary peak position at low *q*, are similar to the data obtained from the TEM images (Table 3).

Gelation of PS-*b*-PAPTES-*b*-PS Films

Cross-linking of the inner PAPTES block was performed through the hydrolysis–condensation of the ethoxysilyl groups in acidic medium by immersing the PS-*b*-PAPTES-*b*-PS films in 1 mol L^{-1} aqueous solution of HCl for 24 h. As previously described for PAPTES-*b*-PS diblock copolymer micelles,[18] hydrolysis–condensation reactions of the ethoxysilyl groups can be qualitatively confirmed by FTIR and NMR spectroscopies. As examples, the FTIR spectra of the $PS_{272}PAPTES_{130}PS_{268}$ sample before and after cross-linking of the PAPTES block are reported in the Supporting Information Figure S3. The copolymer exhibits vibration bands assigned to silyloxy groups (Si—O—C) at around 1100 cm^{-1} and ethoxy groups

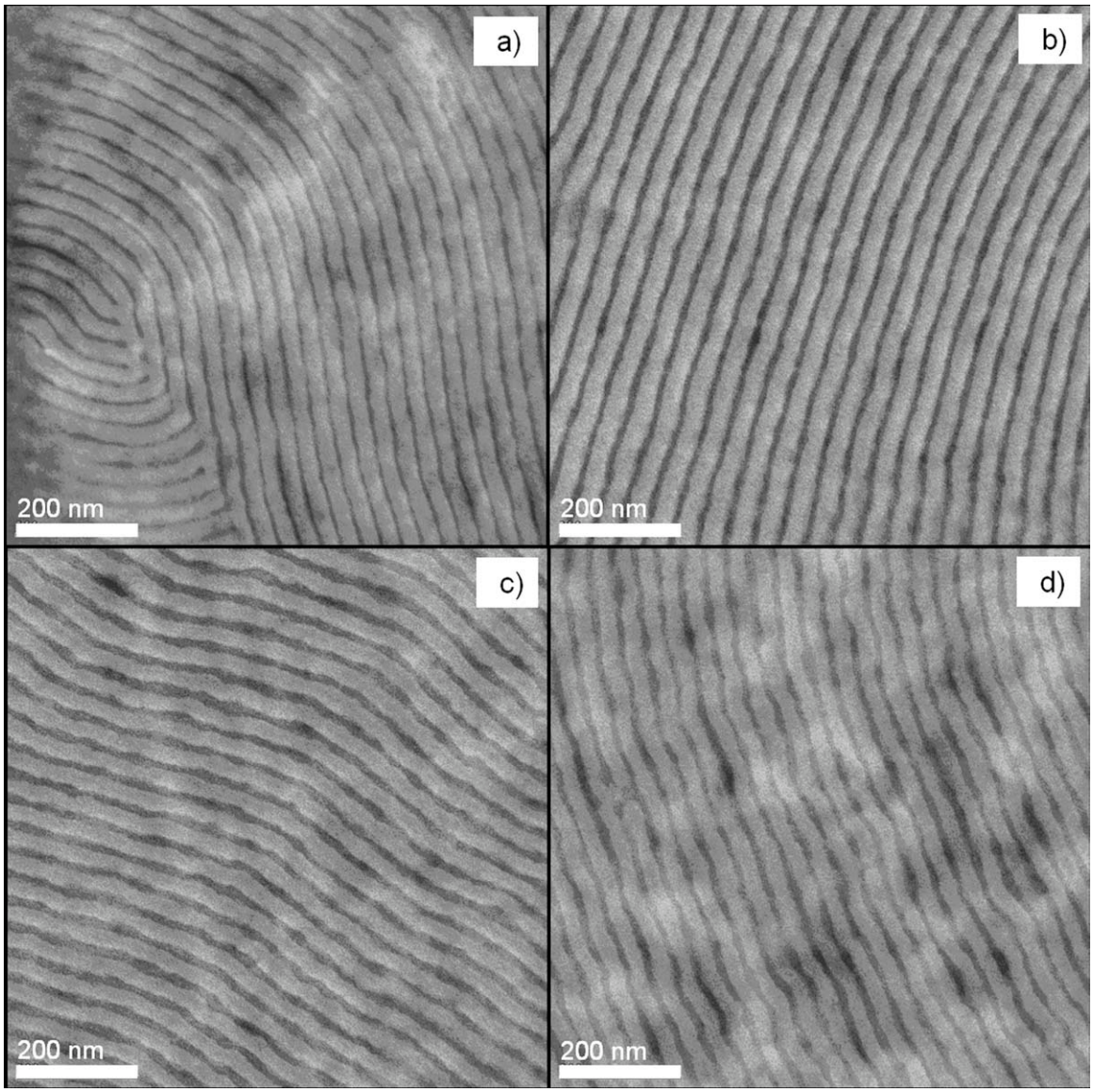

FIGURE 2 TEM micrographs of the PS-*b*-PAPTES-*b*-PS triblock copolymer self-assembled thin films: (a) $PS_{272}PAPTES_{130}PS_{268}$, (b) $PS_{272}PAPTES_{224}PS_{260}$, (c) $PS_{272}PAPTES_{290}PS_{293}$, and (d) $PS_{272}PAPTES_{336}PS_{269}$ (annealed at 150 °C for 72 h).

at 1169 and 961 cm^{-1} [Supporting Information Fig. S3(a)]. On hydrolysis of the ethoxysilyl groups, the latter peaks disappeared while a new strong and wide OH stretching vibration band corresponding to physisorbed water and hydrogen-bonded silanols appeared in the 3700–3150 cm^{-1} region attesting for hydrolysis [Supporting Information Fig. S3(b)]. In addition, a characteristic vibration of the siloxane linkage [ν_{SiOSi}, 1127–1009 cm^{-1}, Supporting Information Fig. S3(b)] provided clear evidence for successful condensation reactions.

The ^{29}Si solid-state NMR spectra of the $PS_{272}PAPTES_{130}PS_{268}$ film before and after the hydrolysis–condensation are presented in Supporting Information Figure S4. Before the addition of the HCl/water solution, the ^{29}Si NMR spectrum [Supporting Information Fig. S4(a)] reveals one major resonance at −45 ppm corresponding to APTES silicon atoms (T^{00}, Table 5). The corresponding solid-state ^{29}Si NMR spectrum under acidic conditions is reported in Supporting Information Figure S4(b), and is not characteristic of a fully condensed material. The spectrum presents two main resonances at −50 and −60 ppm and a weak resonance at −42 ppm. According to the literature,[18,54,55] the first two signals are assigned to T^1 and T^2 species, respectively whereas

TABLE 3 *d*-Spacing Values for Different PS-*b*-PAPTES-*b*-PS Triblock Copolymers

Sample	d_{TEM} (nm)	d_{SAXS} (nm)
$PS_{272}PAPTES_{130}PS_{268}$	34.3	40.7
$PS_{272}PAPTES_{224}PS_{260}$	47.2	52.4
$PS_{272}PAPTES_{290}PS_{293}$	55.8	61.7
$PS_{272}PAPTES_{336}PS_{269}$	51.4	56.1

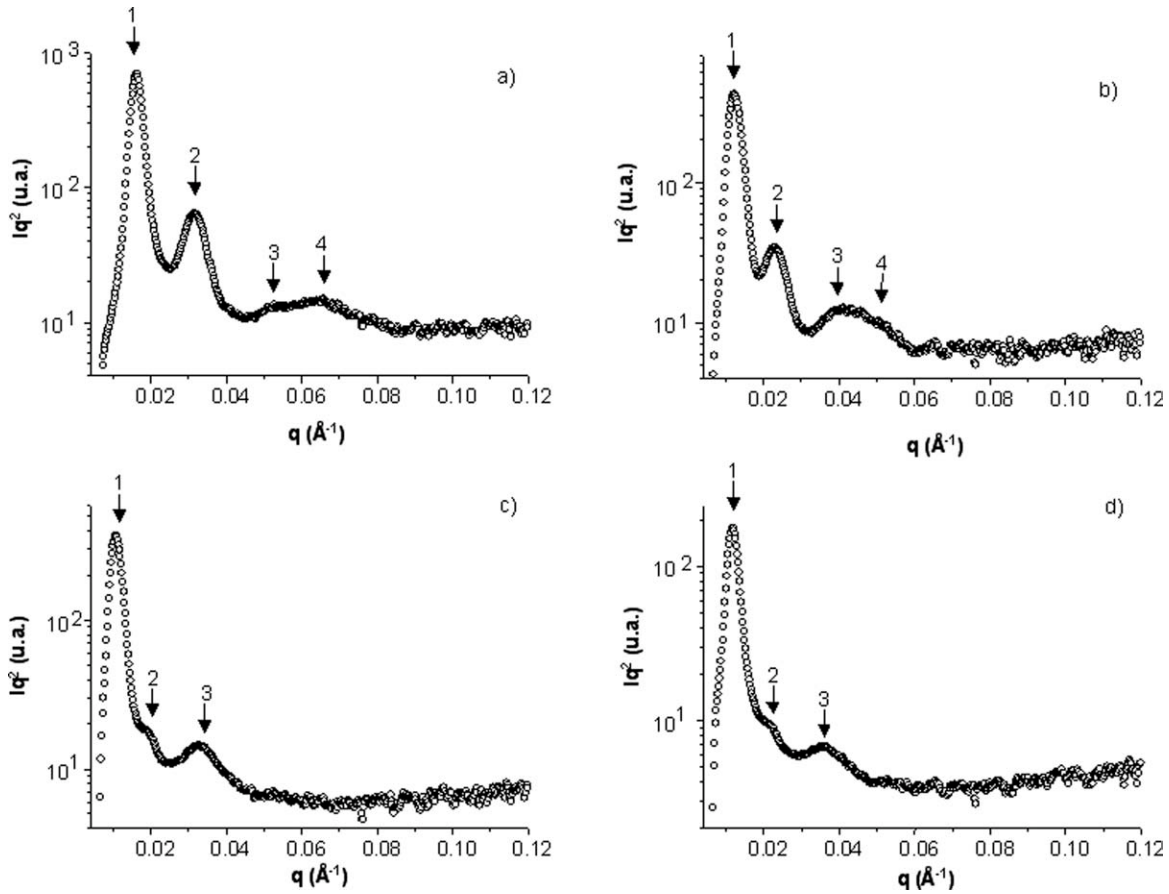

FIGURE 3 SAXS curves of the films obtained from the different copolymers: (a) $PS_{272}PAPTES_{130}PS_{268}$, (b) $PS_{272}PAPTES_{224}PS_{260}$, (c) $PS_{272}PAPTES_{290}PS_{293}$, and (d) $PS_{272}PAPTES_{336}PS_{269}$ after annealing at 150 °C for 72 h.

the third signal corresponds to T^{03} species. Condensation is however incomplete as attested by the predominance of T^1 peaks in the ^{29}Si NMR spectrum and the absence of T^3 signal. Steric hindrance may retard condensation by preventing the silanol groups from coming into a sufficiently close proximity to react. The thermal properties of the PS-*b*-PAPTES-*b*-PS films after the sol–gel reaction were characterized by DSC and TGA. Supporting Information Figure S1 clearly indicates that the T_gs of the triblock copolymers are modified due to cross-linking of the ethoxysilyl groups. The T_g of the PAPTES block disappeared after acidic treatment due to a significant restriction in the chain mobility subsequently to ethoxysilyl cross-linking (Supporting Information Fig. S1). Besides, the upward shift of T_g of the hard PS segment (around 7–10 °C; Table 2) suggests the formation of a siloxane network.[56,57] Figure 4 shows the TGA curves of the $PS_{272}PAPTES_{130}PS_{268}$ and $PS_{272}PAPTES_{290}PS_{293}$ samples before and after the hydrolysis–condensation. After acidic treatment, the PS-*b*-PAPTES-*b*-PS films exhibit a greater resistance to heat than that of the native triblock copolymers. A difference of 10 to 40 °C is observed for the temperature at which maximum weight loss occurred when increasing the PAPTES content from 39.4 to 62.7% (Table 4). This improvement in heat stability may be due to cross-linking of the PAPTES domains.[58,59] To further confirm the hybrid structure, the silica content of the acidic-treated triblock copolymers films was determined by TGA from the residual weight loss after removing the organic polymer by calcination at 800 °C under argon. As expected, the silica content of the hybrid materials increases with increasing the PAPTES content in the triblock copolymer (Table 4). Moreover, as shown in the SEM image of the $PS_{272}PAPTES_{130}PS_{268}$ sample (Fig. 5), the lamellar shape was retained after calcination with a *d*-spacing close to that of the corresponding hybrid film. The temperature dependence of the dynamic mechanical properties of the $PS_{272}PAPTES_{130}PS_{268}$ sample before and after the hydrolysis–condensation is reported in Figure 6. Figure 6(a,b) shows the plots of the storage modulus (G') and loss tangent (tan δ) versus temperature, respectively, in the temperature ranges from −120 to 160 °C. Before acidic treatment, all four triblock copolymers show two α relaxation temperatures in agreement with DSC results. As illustrated for the $PS_{272}PAPTES_{130}PS_{268}$ sample, the first α relaxation temperature at −53.8 °C is attributed to the glass transition within the PAPTES phase followed by a rubbery plateau [Fig. 6(a)]. Then, a drop in G' and an increase in tan δ are observed. This latter native transition can be attributed to the glass transition of the PS nanophase. However, the mechanical behavior of the film at temperatures up to 100 °C does not enable the determination of the corresponding relaxation temperature. The relaxation temperatures

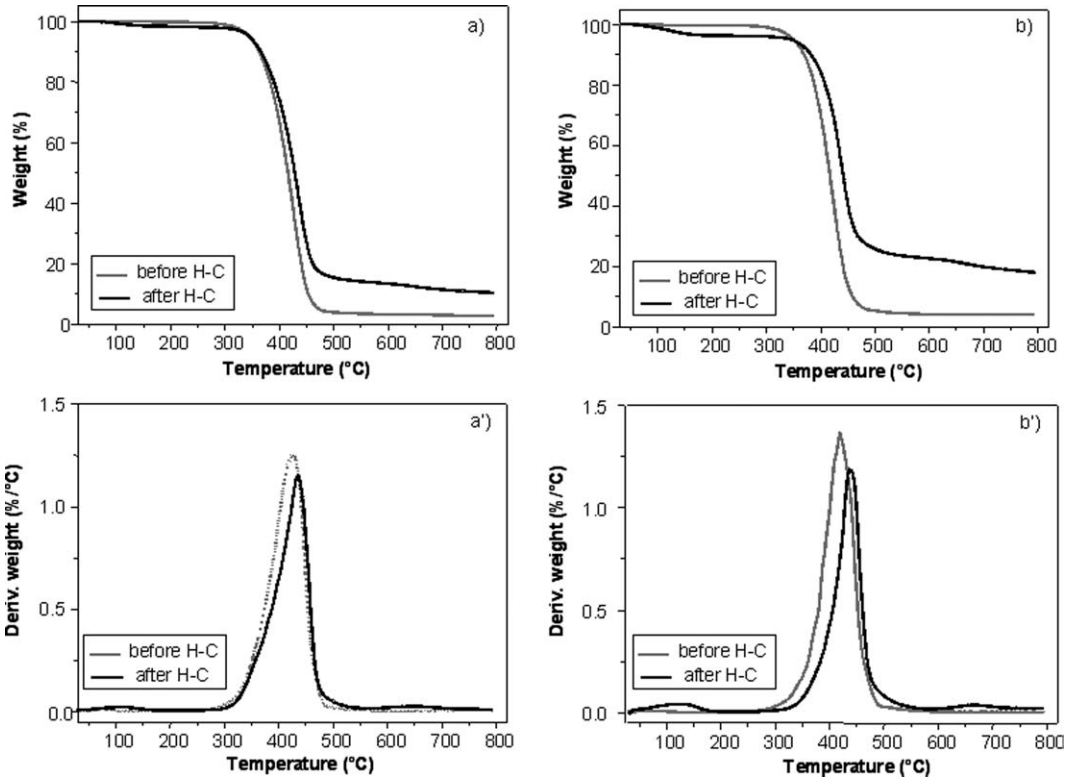

FIGURE 4 TGA curves of (a) $PS_{272}PAPTES_{130}PS_{268}$ and (b) $PS_{272}PAPTES_{290}PS_{293}$ before and after the hydrolysis–condensation (H–C) and their associated first derivates (a′ and b′).

of the PAPTES phase increase by increasing the PAPTES volume fraction in the triblock copolymer (Table 5). After the hydrolysis–condensation reaction, a significant change in the dynamics of PAPTES is visible from the tan δ versus temperature plot in Figure 6(b). A broadening of the tan δ peak, a decrease in tan δ peak height (tan δ_{max}), and a shift from -53.8 to -27.5 °C are observed, suggesting restricted movement of the PAPTES block due to sol–gel cross-linking.[60] It should be mentioned that $T_{\alpha\text{-PAPTES}}$ is not observed after hydrolysis–condensation reactions in the PAPTES-rich sample. For all samples, there is a great difference between the relaxation temperature of the PAPTES nanophase measured by DMA and the glass transition temperature determined by DSC (Table 2), as previously described.[44,61] However, both methods are in qualitative agreement. Moreover, the mechanical properties of the hybrid films are improved which allows the determination of the relaxation temperature of the PS nanophase [e.g., 117.7 °C, Fig. 6(b) and Table 5]. The storage modulus G' significantly increases in the temperature range from -120 to 100 °C [Fig. 6(a)]. Table 6 reports the storage modulus (G') at the glassy plateau for all four PS-*b*-PAPTES-*b*-PS triblock copolymers before and after acidic treatment. Before the hydrolysis–condensation, the storage modulus (G') at the glassy plateau decreases from 2600 to 500 MPa by increasing the PAPTES content from 39.4 to 62.7%, as expected. A significant increase in the modulus is observed for the acidic-treated triblock copolymers. In comparison with the virgin samples, it increases by a factor of 1.6 to 4.3 depending on the PAPTES volume fraction which can be attributed to the formation of siloxane bonds between the PAPTES blocks (Table 6). In

TABLE 4 Residual Weight Loss of PS-*b*-PAPTES-*b*-PS Triblock Copolymers at 800 °C Before and After the Hydrolysis–Condensation Determined by TGA

		Before Hydrolysis–Condensation		After Hydrolysis–Condensation	
Sample	PAPTES (vol %)	T_d (°C)	Residual Fraction (wt %)	T_d (°C)	Polysiloxane (wt %)
$PS_{272}PAPTES_{130}PS_{268}$	39.4	422	2.4	433	10.1
$PS_{272}PAPTES_{224}PS_{260}$	53.2	421	2.7	435	14.2
$PS_{272}PAPTES_{290}PS_{293}$	58.1	418	3.8	435	17.8
$PS_{272}PAPTES_{336}PS_{269}$	62.7	410	4.5	449	18.3

FIGURE 5 SEM micrograph of the $PS_{272}PAPTES_{130}PS_{268}$ hybrid film after calcination at 800 °C.

addition, a β relaxation temperature is observed at −100 °C suggesting secondary relaxations of the condensed PAPTES network. Thus, the dynamic mechanical properties of the PS-*b*-PAPTES-*b*-PS copolymers are significantly changed after sol–gel cross-linking with an increase in G' and T_g.

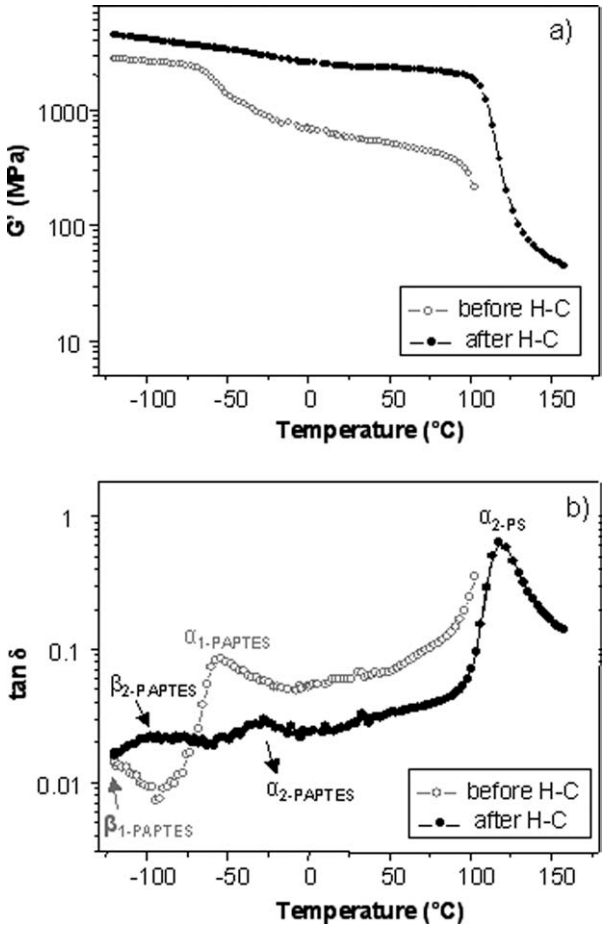

FIGURE 6 Temperature dependence at 5 Hz of (a) G' and (b) tan δ for the $PS_{272}PAPTES_{130}PS_{268}$ copolymer before and after the hydrolysis–condensation (H–C).

CONCLUSIONS

Well-defined PS-*b*-PAPTES-*b*-PS triblock copolymers with molecular weights varying from 88,000 to 139,000 g mol^{-1} and various composition distributions were synthesized by NMP. DSC analysis indicated the presence of two clear glass transition temperatures in the copolymers as a result of microphase separation. TEM observations showed uniform lamellar structures regardless of the composition distribution. The SAXS and TEM analysis provided evidence for the expansion of the interlamellar distance on increasing the PAPTES block length, while maintaining the PS block size constant. Cross-linking of the PAPTES block was performed in acidic medium and monitored by FTIR and ^{29}Si NMR. These techniques enabled to qualitatively assess the extent of the hydrolysis–condensation of the reactive triethoxysilyl side groups. The condensation reaction was incomplete due to steric hindrance. All the acidic-treated triblock copolymers reported in this work showed enhanced mechanical properties as evidenced by an increase in the dynamic storage modulus and a shift of the glass transition temperature toward higher temperatures.

In a future work, the effect of the PS block length of these PAPTES-based triblock copolymers on the mechanical and transport properties will be investigated as well as the

TABLE 5 Glass Transition Relaxation Temperatures at 5 Hz of a Series of PS-*b*-PAPTES-*b*-PS Triblock Copolymers Before and After the Hydrolysis–Condensation (H–C) Determined by DMA

Sample	PAPTES (vol %)	$T_{\alpha\text{-PAPTES}}$ (Before H–C; °C)	$T_{\alpha\text{-PAPTES}}$ (After H–C; °C)	$T_{\alpha\text{-PS}}$ (Before H–C; °C)	$T_{\alpha\text{-PS}}$ (After H–C; °C)
$PS_{272}PAPTES_{130}PS_{268}$	39.4	−53.8	−27.5	N/D	117.7
$PS_{272}PAPTES_{224}PS_{260}$	53.2	−56.0	−32.2	N/D	116.3
$PS_{272}PAPTES_{290}PS_{293}$	58.1	−52.0	−35.4	N/D	111.5
$PS_{272}PAPTES_{336}PS_{269}$	62.7	−46.6	–	N/D	113.2

N/D: not determined.

TABLE 6 Values of the Storage Modulus (G') at the Glassy Plateau, that is, at $T < T_{\alpha\text{-PAPTES}}$, of a Series of PS-*b*-PAPTES-*b*-PS Triblock Copolymer Films Before and After the Hydrolysis–Condensation (H–C)

Sample	PAPTES (vol %)	$G'_{\text{before H–C}}$ (MPa)	$G'_{\text{after H–C}}$ (MPa)	$G'_{\text{after H–C}}/G'_{\text{before H–C}}$
$PS_{272}PAPTES_{130}PS_{268}$	39.4	~2,600	~4,050	1.6
$PS_{272}PAPTES_{224}PS_{260}$	53.2	~1,350	~3,900	2.9
$PS_{272}PAPTES_{290}PS_{293}$	58.1	~1,200	~3,550	3.0
$PS_{272}PAPTES_{336}PS_{269}$	62.7	~500	~2,150	4.3

potential of these PAPTES-based diblock or triblock copolymers as surface modification agents of colloidal silica particles to obtain functional hybrid colloids.

REFERENCES AND NOTES

1 Du, J.; Armes, S. P. J Am Chem Soc 2005, 127, 12800–12801.

2 Bartholome, C.; Beyou, E.; Bourgeat-Lami, E.; Chaumont, P.; Zydowicz, N. Macromolecules 2005, 38, 1099–1106.

3 Bartholome, C.; Beyou, E.; Bourgeat-Lami, E.; Chaumont, P.; Zydowicz, N. Polymer 2005, 46, 8502–8510.

4 Bailly, B.; Donnenwirth, A.-C.; Bartholome, C.; Beyou, E.; Bourgeat-Lami, E. J Nanomater 2006, 2006, 1–10.

5 Huo, Q.; Liu, J.; Wang, L.-Q.; Jiang, Y.; Lambert, T. N.; Fang, E. J Am Chem Soc 2006, 128, 6447–6453.

6 Wang, H.; Wang, Y.; Zhou, X.; Zhou, L.; Tang, J.; Lei, J.; Yu, C. Adv Funct Mater 2007, 17, 613–617.

7 Shimura, N.; Ogawa, M. Bull Soc Chim Jpn 2005, 78, 1154–1159.

8 Smatt, J. H.; Schunk, S.; Linden, M. Chem Mater 2003, 15, 2354–2361.

9 Akbar, S.; Beyou, E.; Cassagnau, P.; Chaumont, P. Mater Chem Phys 2009, 117, 482–488.

10 Du, L.; Liao, S.; Khatib, H. A.; Stoddart, J. F.; Zink, J. I. J Am Chem Soc 2009, 131, 15136–15142.

11 Guerrero-Martinez, A.; Perez-Juste, J.; Liz-Marzan, L. M. Adv Mater 2010, 22, 1182–1195.

12 Kim, J.; Kim, H. S.; Lee, L.; Kim, T.; Kim, H.; Yu, T.; Song, I. C.; Moon, W. K.; Hyeon, T. Angew Chem Int Ed 2008, 47, 8438–8444.

13 Gohy, J. F. Adv Polym Sci 2005, 190, 65–136.

14 Willet, N.; Gohy, J.-F.; Auvray, L.; Varshney, S.; Jerome, R.; Leyh, B. Langmuir 2008, 24, 3009–3015.

15 Brinker, C.; Scherer, G. Sol–Gel Science: The Physics and Chemistry of Sol–Gel Processing; Academic Press: Boston, 1990.

16 Negrete-Herrera, N.; Letoffe, J.-M.; Reymond, J.-P.; Bourgeat-Lami, E. J Mater Chem 2005, 15, 863–871.

17 Yu, Y.-Y.; Chen, W.-C. Mater Chem Phys 2003, 82, 388–395.

18 Gamys, C. G.; Beyou, E.; Bourgeat-Lami, E. J Polym Sci Part A: Polym Chem 2010, 48, 784–793.

19 Zhou, J. F.; Wang, L.; Dong, X. C.; Yang, Q.; Wang, J.; Yu, H.; Chen, X. Eur Polym J 2007, 43, 1736–1743.

20 Du, J.; Chen, Y.; Zhang, Y.; Han, C. C.; Fischer, K.; Schmidt, M. J Am Chem Soc 2003, 125, 14710–14711.

21 Du, J.; Chen Y. Macromolecules 2004, 37, 5710–5716.

22 Du, J.; Chen Y. Macromol Rapid Commun 2005, 26, 491–494.

23 Zhang, K.; Yu, X.; Gao, L.; Chen, Y.; Yang, Z. Langmuir 2008, 24, 6542–6548.

24 Zhang, K.; Gao, L.; Chen, Y. Macromolecules 2008, 41, 1800–1807.

25 Simon, P. F. W.; Ulrich, R.; Spiess, H. W.; Wiesner, U. Chem Mater 2001, 13, 3464–3486.

26 Hayward, R. C.; Chmelka, B. F.; Kramer, E. J. Adv Mater 2005, 17, 2591–2598.

27 Hadjichristtidis, N.; Iatrou, H.; Pitsikalis, M.; Pipas, S.; Avgeropoulos, A. Prog Polym Sci 2005, 30, 725–782.

28 Erhardt, R.; Boker, A.; Zettl, H.; Kaya, H.; Pyckhout-Hintzen, W.; Krausch, G. Macromolecules 2001, 34, 1069–1075.

29 Erhardt, R.; Zhang, M. F.; Böker, A.; Zettl, H.; Abetz, C.; Frederik, P. J Am Chem Soc 2003, 125, 3260–3267.

30 Liu, Y. F.; Abetz, V.; Müller, A. H. E. Macromolecules 2003, 36, 7894–7898.

31 Walther, A.; André, X.; Drechsler, M.; Abetz, V.; Müller, A. H. E. J Am Chem Soc 2007, 129, 6187–6198.

32 Yan, X. H.; Liu, F. T.; Li, Z.; Liu, G. J. Macromolecules 2001, 34, 9112–9116.

33 Walther, A.; Drechsler, M.; Müller, A. H. E. Soft Matter 2009, 5, 385–390.

34 Xu, H.; Erhardt, R.; Abetz, V.; Müller, A. H. E.; Gödel, W. A. Langmuir 2001, 17, 6787–6793.

35 Walther, A.; Hoffmann, M.; Müller, A. H. E. Angew Chem Int Ed 2008, 47, 711–714.

36 Zhang, K.; Gao, L.; Zhang, C.; Chen, Y. J Mater Chem 2009, 19, 3482–3489.

37 Zhang, K.; Gao, L.; Chen, Y. Polymer 2010, 51, 2809–2817.

38 Mc Hale, R.; Ghasdian, N.; Hondow, N. S.; Richardson, P. M.; Voice, A. M.; Brydson, R.; Wang, X. Macromolecules, 2010, 43, 6343–6347.

39 Matsushita, Y.; Nomura, M.; Watanabe, J.; Mogi, Y.; Noda, I.; Imai, M. Macromolecules, 1995, 28, 6007–6013.

40 Nandan, B. J Polym Sci Part B: Polym Phys 2010, 48, 1594–1605.

41 Ozaki, H.; Hirao, A.; Nakahama, S. Macromolecules 1992, 25, 1391–1395.

42 Xiong, M.; Zhang, K.; Chen, Y. Eur Polym J 2008, 44, 3835–3841.

43 Robin, S.; Gnanou, Y. Macromol Symp 2001, 165, 43–53.

44 Phan, T. N. T.; Maiez-Tribut, S.; Pascault, J. P.; Bonnet, A.; Gerard, P.; Guerret, O.; Bertin, D. Macromolecules 2007, 40, 4516–4523.

45 Robin, S.; Guerret, O.; Couturier, J.-L.; Pirri, R.; Gnanou, Y. Macromolecules 2002, 35, 3844–3848.

46 Bothe, M.; Schmidt-Naake, G. Macromol Chem Phys 2004, 205, 208–216.

47 Riess, G. Prog Polym Sci 2003, 28, 1107–1170.

48 Siebert, M.; Albrecht, K.; Spiertz, R.; Keul, H.; Möller, M. Soft Matter 2011, 7, 587–594.

49 Bates, F. S.; Fredrickson, G. H. Annu Rev Phys Chem 1990, 41, 525–557.

50 Helfand, E.; Wasserman, Z. R. Macromolecules, 1976, 9, 879–888.

51 Kampf, G.; Hoffmann, M.; Kromer, H. Ber Bunsenges Phys Chem 1970, 74, 851–852.

52 Hoffmann, M. Makromol Chem 1971, 144, 301–305.

53 Gao, L.; Yao, J.; Shen, Z.; Wu, Y.; Chen, X.; Fan, X.; Zhou, Q. Macromolecules, 2009, 42, 1047–1050.

54 Loy, D. A.; Baugher, B. M.; Baugher, C. R.; Scneider, D. A.; Rahimian, K. Chem Mater 2000, 12, 3624–3632.

55 Young, S. K.; Jarrett, W. L.; Mauritz, K. A. Polymer 2002, 43, 2311–2320.

56 Costa, R. O. R.; Vasconcelos, W. L. J Non-Cryst Solids 2002, 304, 84–91.

57 Chan, C.-K.; Chu, I. M. Polymer 2001, 42, 6823–6831.

58 Hsiue, G.-H.; Kuo, W.-J.; Huang, Y.-P.; Jeng, R.-J. Polymer 2000, 41, 2813–2825.

59 Shang, X.-Y.; Zhu, Z.-K.; Yin, J.; Ma, X.-D. Chem Mater 2002, 14, 71–77.

60 Patel, S.; Bandyopadhyay, A.; Vijayabaskar, V.; Bhowmick, A. K. Polymer, 2005, 46, 8079–8090.

61 Kozlowska, A.; Majszczyk, J.; Orlowski, M. Rev Adv Mater Sci 2006, 12, 160–165.